

# Beyond Time-Dependent Density Functional Theory Using Only Single Excitations: Methods for Computational Studies of Excited States in Complex Systems

John M. Herbert,\* Xing Zhang, Adrian F. Morrison, and Jie Liu<sup>†</sup>

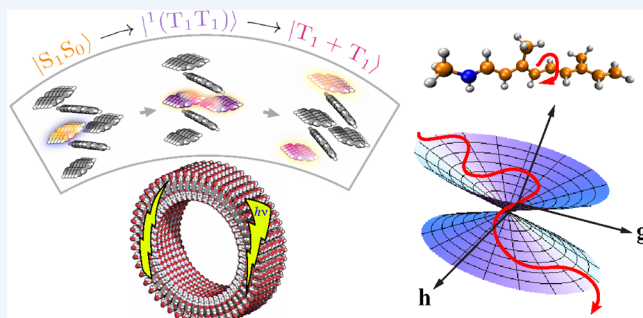
Department of Chemistry and Biochemistry, The Ohio State University, Columbus, Ohio 43210, United States

**CONSPECTUS:** Single-excitation methods, namely, configuration interaction singles and time-dependent density functional theory (TDDFT), along with semiempirical versions thereof, represent the most computationally affordable electronic structure methods for describing electronically excited states, scaling as  $O(N_{\text{atoms}}^4)$  absent further approximations. This relatively low cost, combined with a treatment of electron correlation, has made TDDFT the most widely used excited-state quantum chemistry method over the past 20+ years. Nevertheless, certain inherent problems (beyond just the accuracy of this or that exchange-correlation functional) limit the utility of traditional TDDFT. For one, it affords potential energy surfaces whose topology is incorrect in the vicinity of any conical intersection (CI) that involves the ground state. Since CIs are the conduits for transitions between electronic states, the TDDFT description of photochemistry (internal conversion and intersystem crossing) is therefore suspect. Second, the  $O(N_{\text{atoms}}^4)$  cost can become prohibitive in large systems, especially those that involve multiple electronically coupled chromophores, for example, the antennae structures of light-harvesting complexes or the conjugated polymers used in organic photovoltaics. In such cases, the smallest realistic mimics might already be quite large from the standpoint of *ab initio* quantum chemistry. This Account describes several new computational methods that address these problems.

Topology around a CI can be rigorously corrected using a “spin-flip” version of TDDFT, which involves an  $\alpha \rightarrow \beta$  spin-flipping transition in addition to occupied  $\rightarrow$  virtual excitation of one electron. Within this formalism, singlet states are generated via excitation from a high-spin triplet reference state, doublets from a quartet, etc. This provides a more balanced treatment of electron correlation between ground and excited states. Spin contamination is problematic away from the Franck–Condon region, but we describe a “spin-complete” version of the theory in which proper spin eigenstates are obtained by construction.

For systems of coupled chromophores, we have developed an *ab initio* version of the Frenkel–Davydov exciton model in which collective excitations of the system are expanded in a basis of excited states computed for individual chromophores. The monomer calculations are trivially parallelizable, as is computation of the coupling matrix elements needed to construct the exciton Hamiltonian, and systems containing hundreds of chromophores can be tackled on commodity hardware. This enables calculations on organic semiconductors, where even small model systems exhibit a semicontinuum of excited states that renders traditional TDDFT computationally challenging. Despite including only single excitations on each monomer, the exciton model can describe entangled spins on two or more monomers, an effect that is responsible for excitation energy transfer between chromophores, for example, in singlet fission.

Excitonic approximations can also be applied to the TDDFT equations themselves, and a particularly promising application is to describe the effects of environment on an excitation that is localized on a single chromophore. This “local excitation approximation” to TDDFT allows an essentially arbitrary number of solvent molecules to be included in the calculation in a highly parallelizable way such that the time-to-solution increases only very slowly as additional solvent molecules are added. It is therefore possible to converge the calculation with respect to describing an ever-larger portion of the environment at a quantum-mechanical level.



## 1. INTRODUCTION

The conceptual picture of an electronic excitation as a single-particle transition between an occupied molecular orbital (MO) and an unoccupied or “virtual” MO is—to misquote H. L. Mencken<sup>1</sup>—neat, plausible, and *not entirely wrong*. The more educated quantum mechanic realizes, of course, that an excited state  $|\psi^*\rangle$  should be expressed as a linear combination of single excitations,

$$|\psi^*\rangle = \sum_i \sum_a t_{ia} |\Phi^{ia}\rangle \quad (1)$$

Here,  $|\Phi^{ia}\rangle$  is a Slater determinant formed from ground-state MOs, removing an electron from occupied orbital  $i$  and placing it

Received: January 26, 2016

Published: April 21, 2016

into virtual orbital  $a$ . The *ansatz* in eq 1 is used in the simplest excited-state quantum chemistry model, configuration interaction singles (CIS), but also in the most widely-used model, time-dependent density functional theory (TDDFT).<sup>2</sup> The latter is popular due to its relatively low cost and generally reasonable accuracy, with errors  $\lesssim 0.3$  eV for vertical excitation energies in many cases.<sup>3,4</sup>

On the other hand, eq 1 is fundamentally incapable of describing states characterized by a double excitation out of the ground state. These are important, for example, to describe the “multi-exciton” state of relevance to singlet fission,<sup>5</sup> in which triplet excited states on two different molecules spin-couple to an overall singlet. Double excitations are also crucial for obtaining a balanced description of the conical intersections that are responsible for photochemistry.<sup>6</sup> Nevertheless, the aim of this Account is to explore how far one can go with variations on the single-excitation *ansatz*.

For application to photochemical reactions, the accuracy of TDDFT is compelling, yet until recently there were fundamental limitations in the description of TDDFT potential energy surfaces in regions associated with breakdown of the Born–Oppenheimer (BO) approximation. Some of these deficiencies have been rectified recently,<sup>7,8</sup> using the “spin-flip” approach to TDDFT,<sup>10</sup> providing a low-cost *ab initio* method for computational photochemistry.

In systems with multiple chromophores, the cost of traditional single-excitation approaches may become prohibitive. Examples include collective excitations in systems such as organic semiconductors (of interest in photovoltaics), where the excited-state wave functions delocalize across more than one monomer. Even in cases where the excitation is localized, it might still be necessary to describe an extended portion of the environment at a quantum-mechanical level in order to obtain converged excitation energies. We will describe new models that significantly reduce the cost of excited-state calculations in systems such as these, by exploiting the *ansatz* in eq 1 but applied separately to individual subsystems.

## 2. PHOTOCHEMISTRY

### 2.1. Conical Intersections

Theoretical photochemistry is the study of the nonadiabatic events that govern internal conversion and intersystem crossing. These occur when at least two potential energy surfaces become (quasi)degenerate, leading to a breakdown of the BO approximation such that coupling between nuclear and electronic degrees of freedom must be considered. Transitions between adiabatic BO states  $|\psi_j\rangle$  are driven by matrix elements of the nuclear position derivatives, as codified in the first-order derivative coupling vector

$$\mathbf{d}_{JK} = \langle \psi_j | (\partial / \partial \mathbf{R}) | \psi_K \rangle \quad (2)$$

A related quantity is the nonadiabatic coupling vector

$$\begin{aligned} \mathbf{h}_{JK} &= \langle \psi_j | (\partial \hat{H} / \partial \mathbf{R}) | \psi_K \rangle \\ &= (E_K - E_J) \mathbf{d}_{JK} \end{aligned} \quad (3)$$

where  $\hat{H}$  is the electronic Hamiltonian.

Consider the matrix representation of  $\hat{H}$  in a basis of two arbitrary electronic states:

$$\mathbf{H} = \begin{pmatrix} H_{00}(\mathbf{R}) & H_{01}(\mathbf{R}) \\ H_{01}^*(\mathbf{R}) & H_{11}(\mathbf{R}) \end{pmatrix} \quad (4)$$

The BO states diagonalize  $\mathbf{H}$ , and two conditions must be satisfied in order to obtain degeneracy in the BO representation:  $H_{00} = H_{11}$  and  $H_{01} = 0$ . As such, degeneracies between two BO states exist in subspaces of dimension  $N_{\text{int}} - 2$ , where  $N_{\text{int}} = 3N_{\text{atoms}} - 6$  is the number of internal (vibrational) degrees of freedom. This  $(N_{\text{int}} - 2)$ -dimensional subspace is known as the *seam space*.<sup>12,13</sup> In the remaining two degrees of freedom, known as the *branching space*, the degeneracy between BO states is lifted by an infinitesimal displacement. In three dimensions, this resembles a double cone about the point of intersection, as shown in Figure 1a, and such points are therefore known as *conical intersections* (CIs). The branching space is defined by a pair of vectors  $\mathbf{g}_{JK}$  and  $\mathbf{h}_{JK}$ , where<sup>12,13</sup>

$$\mathbf{g}_{JK} = \frac{\partial E_J}{\partial \mathbf{R}} - \frac{\partial E_K}{\partial \mathbf{R}} \quad (5)$$

The topography of potential surfaces near a CI can significantly affect the dynamics.<sup>13–17</sup> The tilt of the CI cone can be characterized based on the projection of the vector

$$\mathbf{s}_{JK} = \frac{1}{2} \left( \frac{\partial E_J}{\partial \mathbf{R}} + \frac{\partial E_K}{\partial \mathbf{R}} \right) \quad (6)$$

onto the branching plane. Define scaled projections

$$s^x = (\mathbf{s}_{JK} \cdot \mathbf{g}_{JK}) / g^2 \quad s^y = (\mathbf{s}_{JK} \cdot \mathbf{h}_{JK}) / h^2 \quad (7)$$

where  $g = \|\mathbf{g}_{JK}\|$  and  $h = \|\mathbf{h}_{JK}\|$ . The CI is “peaked” if  $s^x$  and  $s^y$  are close to zero (Figure 1b); otherwise it is “sloped” (Figure 1d). It is suggested that the former case provides a better “conical funnel”, providing more efficient nonadiabatic transitions.<sup>13–17</sup>

### 2.2. Time-Dependent DFT

The quantity  $\mathbf{g}_{JK}$  is available for any model chemistry for which ground- and excited-state gradients are available. Analytic gradient formalism can be used to obtain  $\mathbf{h}_{JK}$  as well, although this is more complicated and thus nonadiabatic couplings are only available for a few electronic structure models and only in a few quantum chemistry programs. Given that TDDFT often provides reasonable excited-state properties and can routinely be applied to systems with 100+ atoms, it is noteworthy that only recently have analytic derivative couplings been derived and implemented for this method.<sup>7,8,18–20</sup>

A serious drawback for photochemical applications, however, is that TDDFT predicts the wrong topology for any CI that involves the reference state,<sup>6</sup> which is usually the ground state. Excited states in TDDFT are computed from the linear response of the reference-state density,<sup>2</sup> and if one imagines eq 4 as the TDDFT response matrix, then couplings  $H_{0n}$  to the reference state “0” vanish identically. As a result, there is only one degeneracy condition ( $H_{00} = H_{11}$ ); hence the branching space is one-dimensional.<sup>6</sup> Moreover, because electron correlation is treated in an unbalanced way for the reference state compared with the response states, problems arise in cases of symmetry-required degeneracy, such as Jahn–Teller distortion.<sup>7</sup>

The simplest extension of TDDFT that corrects these problems is spin-flip (SF) TDDFT.<sup>10</sup> In this approach, one uses a reference state whose multiplicity is  $S + 1$  in order to target states with multiplicity  $S$ . This involves generating all occupied → virtual excitations of the high-spin  $S + 1$  reference state, in conjunction with an  $\alpha \rightarrow \beta$  spin flip (an example for  $S = 0$  is shown in Figure 2). For  $S = 0$ , this generates a closed-shell determinant that resembles the singlet ground state (Figure 2b), whose excitation energy may be negative if the ground state is a

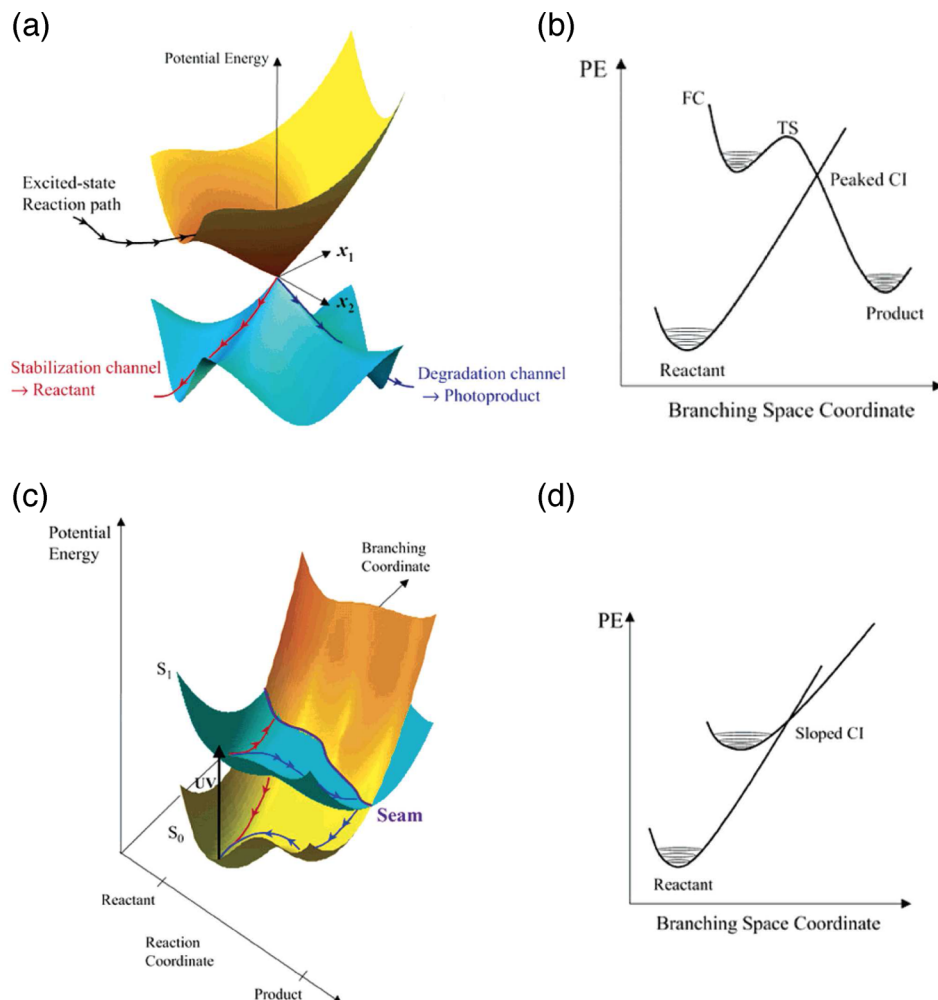


**Figure 1.** CIs between potential surfaces. The two-dimensional branching space defines a double cone, which is most evident in the peaked CI in panel a, yet this is merely one point along the conical seam that is evident in panel c. Panels b and d are one-dimensional cross sections that emphasize the “peaked” nature of the CI in panel a and the “sloped” nature of that in panel c. Reprinted with permission from ref 11. Copyright 2005 American Chemical Society.

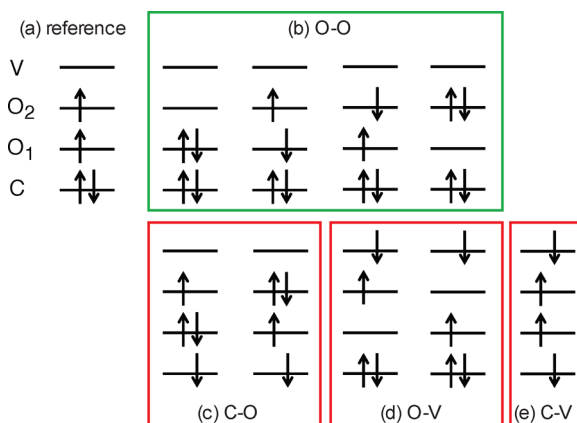


**Figure 2.** (a) High-spin triplet reference state and (b) singlet configurations generated by a spin-flipping excitation, the first of which resembles the singlet ground state. Panels c–e illustrate the additional determinants that are necessary to obtain spin eigenstates. Reprinted with permission from ref 21. Copyright 2015 American Institute of Physics.

singlet. In any case,  $S_0$  is treated in a balanced way alongside  $S_1$ ,  $S_2$ , etc. We have recently derived and implemented analytic derivative couplings ( $\mathbf{h}_{JK}$  vectors) for SF-TDDFT,<sup>7,8</sup> which enables the use of algorithms that greatly accelerate the location and

optimization of CIs, compared with the algorithms that must be used when only analytic gradients ( $\mathbf{g}_{JK}$  vectors) are available.<sup>7</sup> At the time of this writing, analytic derivative couplings for SF-TDDFT are available only in the Q-CHEM code.<sup>9</sup>

A brief comment is in order regarding the choice of density functional for use in SF-TDDFT. In early applications to vertical excitation energies of radicals, SF-TDDFT was found to perform best with functionals containing ~50% Hartree–Fock exchange.<sup>10</sup> This is somewhat more than the 20–25% Hartree–Fock exchange used in hybrid functionals such as B3LYP and PBE0 that are popular for ground-state calculations and traditional TDDFT, for theoretical reasons suggested in ref 22. In most SF-TDDFT studies of CIs,<sup>7,8,21,23–25,29</sup> the “Becke half and-half” (BH&H) functional has been used, which mixes 50% Hartree–Fock exchange with 50% of Becke88 exchange. All SF-TDDFT calculations herein use the BH&HLYP functional, which combines BH&H with Lee–Yang–Parr correlation.

### 2.3. Examples

**2.3.1. Topography and Topology of CIs.** Since the conical seam is a subspace of dimension  $N_{\text{int}} - 2$ , the photochemical analogue of a ground-state minimum-energy pathway usually involves a search for the minimum-energy crossing point (MECP) along the seam, which can then be used as one end point in a pathway search starting from the Franck–Condon

geometry on the excited state. MECPs can be located much more efficiently using algorithms that exploit both the  $\mathbf{g}_{JK}$  and  $\mathbf{h}_{JK}$  vectors as opposed to  $\mathbf{g}_{JK}$  alone.<sup>7</sup>

Figure 3 presents potential scans around two CIs of ethylene, computed using SF-TDDFT. It is clear by inspection that the twisted/pyramidalized MECP (Figure 3a) exhibits a peaked topography whereas the ethylidene MECP (Figure 3b) is sloped. This is confirmed by the values of  $s^x$  and  $s^y$  reported in Table 1.

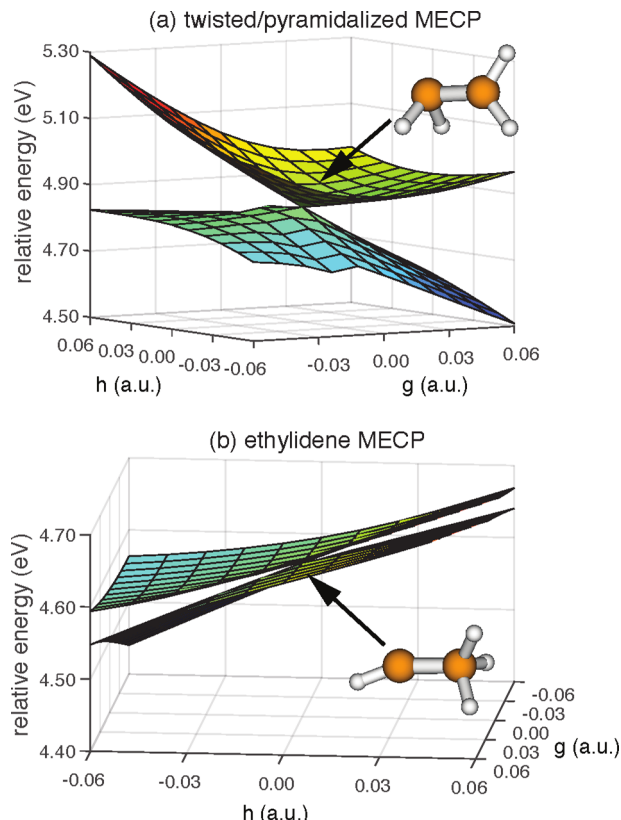


**Figure 3.** MECPs between the  $S_0$  and  $S_1$  states of  $C_2H_4$ , computed using SF-TDDFT at the BH&HLYP/6-31G\*\* level. Energies are relative to the  $S_0$  minimum.

**Table 1. Tilt Parameters for Two MECPs Connecting the  $S_0$  and  $S_1$  States of  $C_2H_4$ , Computed Using Spin-Flipping versus Spin-Conserving TDDFT**

MECP	$ s^x $		$ s^y $	
	spin-flipping <sup>a</sup>	spin-conserving <sup>b</sup>	spin-flipping <sup>a</sup>	spin-conserving <sup>b</sup>
twisted/pyramidalized	0.32	0.27	0.60	35.48
ethylidene	1.36	0.55	3.34	2.73

<sup>a</sup>BH&HLYP/6-31G\*\* functional. <sup>b</sup>PBE0/6-31G\*\* functional.

The picture is very different when the same calculation is carried out using traditional, spin-conserving TDDFT, as shown in Figure 4. Here, degeneracy is lifted in one dimension only, which is most evident for the ethylidene CI (Figure 4b). Not surprisingly, the tilt parameters  $s^x$  and  $s^y$  (Table 1) are quite different in this case and fail to provide even qualitatively correct information about whether the CI is peaked or sloped.

**2.3.2. Photoisomerization.** Retinal protonated Schiff base (RPSB), the chromophore in the rhodopsin family of proteins, converts light into mechanical energy via excited-state *cis* → *trans*

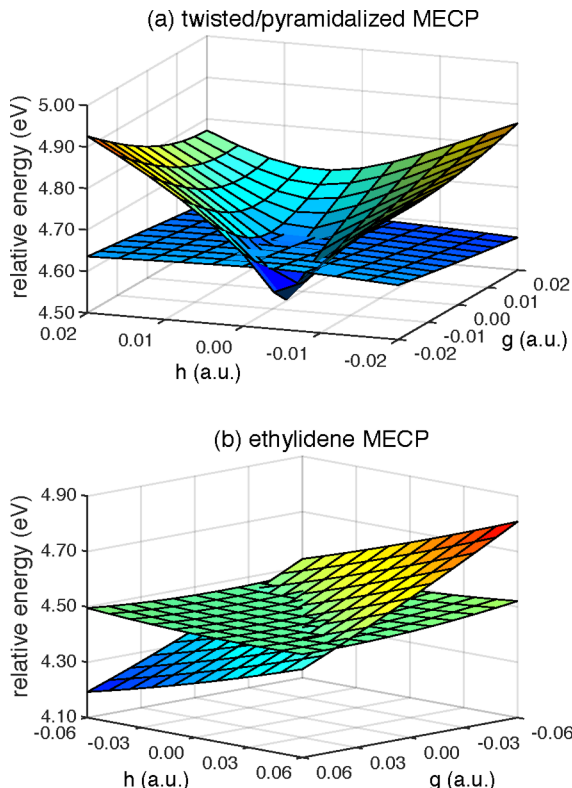


**Figure 4.** MECPs between the  $S_0$  and  $S_1$  states of  $C_2H_4$ , computed using traditional TDDFT at the PBE0/6-31G\*\* level.

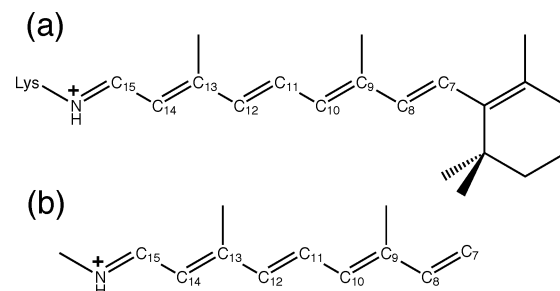


**Figure 5.** Structure of (a) all-*trans* RPSB and (b) the truncated analogue considered here.

isomerization. RPSB has five double bonds capable of isomerization; see Figure 5. In rhodopsin, isomerization occurs exclusively at the  $C_{11}=C_{12}$  bond, while in bacteriorhodopsin the  $C_{13}=C_{14}$  photoisomerization is the dominant reaction.<sup>26</sup> Several photoproducts are obtained in solvated environments, with the 11-*cis* isomer predominating.<sup>27</sup>

To demonstrate the applicability of SF-TDDFT to photochemistry, we examine photoisomerization pathways in a truncated model of the RPSB chromophore, for which CASSCF calculations have been reported.<sup>16</sup> (The entire RPSB chromophore could be studied using SF-TDDFT).

We optimize  $S_0/S_1$  MECPs corresponding to isomerization at  $C_{11}=C_{12}$  and at  $C_{13}=C_{14}$ ; we label these MECPs as  $CI_{11-12}$  and  $CI_{13-14}$ , respectively. Previous work has suggested that SF-TDDFT provides CI structures that are in good agreement with multireference wave function results,<sup>25</sup> and Figure 6 shows that the MECPs obtained here are nearly identical to CASSCF structures. However, SF-TDDFT predicts  $CI_{13-14}$  to be 1 eV higher in energy than  $CI_{11-12}$ , whereas CASSCF predicts them to

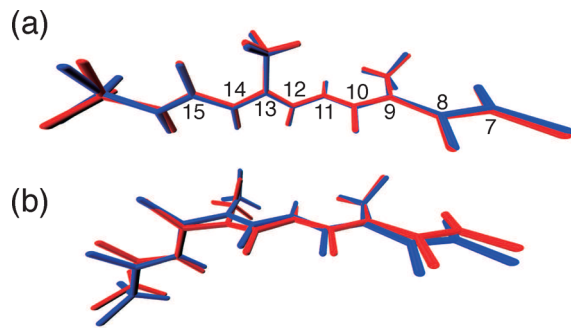


**Figure 6.** MECP structures for the RPSB model in Figure 5b, superimposing CASSCF results (in blue, from ref 16) with SF-TDDFT results (BH&HLYP/6-31G\*, in red) for (a)  $\text{CI}_{11-12}$  and (b)  $\text{CI}_{13-14}$ .

be nearly isoenergetic.<sup>16</sup> Further work is needed to determine whether this is a failure of DFT or rather is due to lack of dynamical correlation in CASSCF, a known problem with the latter method.<sup>28</sup>

Figure 7 summarizes the energy levels of the minima and MECPs along the photoisomerization pathways of the all-*trans* RPSB analogue. Following  $S_0 \rightarrow S_1$  excitation, the system may become trapped in the planar local minimum ( $S_{1\text{min-p}}$ ). Both  $\text{CI}_{11-12}$  and a local minimum with a twisted  $\text{C}_{13}=\text{C}_{14}$  bond ( $S_{1\text{min-13}}$ ) are energetically lower than  $S_{1\text{min-p}}$ . At  $\text{CI}_{11-12}$ , the system may return to  $S_0$  via nonadiabatic transition and further relax on the  $S_0$  surface to form the 11-*cis* isomer. The  $S_{1\text{min-13}}$  minimum, on the other hand, lies below  $\text{CI}_{13-14}$ ; hence the system may become trapped in the excited state. Furthermore, the minimum-energy reaction pathway connecting  $S_{0\text{min}}$  and  $\text{CI}_{11-12}$  is barrierless, while the pathway connecting  $S_{0\text{min}}$  and  $\text{CI}_{13-14}$  has a barrier of 0.3 eV. Overall, our SF-TDDFT calculations suggest that the 11-*cis* isomer of RPSB will be the dominant photoproduct, despite being less stable than the 13-*cis* isomer.

#### 2.4. Spin Contamination

An unfortunate drawback of SF-TDDFT is that it is subject to serious spin contamination, to the point that it frequently becomes difficult to assign spin multiplicities away from the Franck–Condon region.<sup>21,25</sup> For optimization of singlet excited

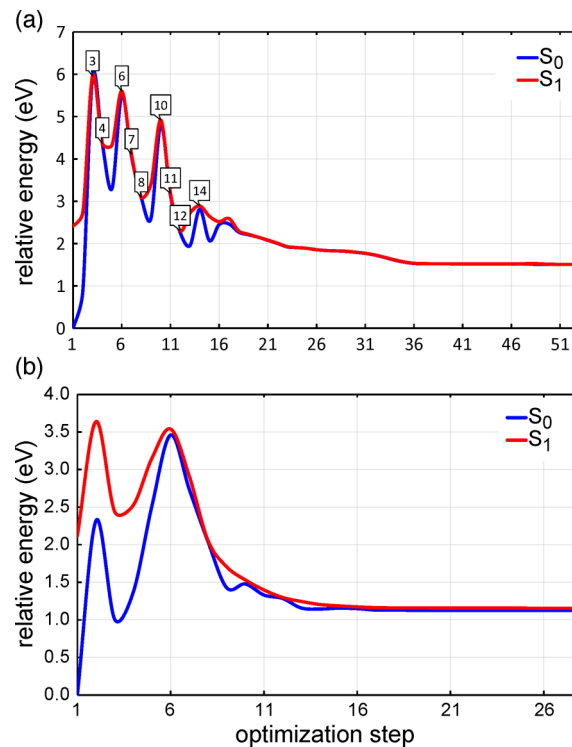


**Figure 8.**  $S_0/S_1$  MECP optimization trajectories for  $\text{C}_2\text{H}_4$  starting from a twisted geometry. (a) SF-TDDFT results, where the numbered labels indicate steps for which the assignment of spin multiplicity is ambiguous. (b) SA-DF-DFT results. All calculations use the BH&HLYP/6-31G\* functional. Reprinted with permission from ref 21. Copyright 2015 American Institute of Physics.

states starting from a triplet reference, we often find that  $\langle \hat{S}^2 \rangle \approx 1$  (in atomic units), indicating a state that is an equal mixture of singlet and triplet. An example is shown in Figure 8a, which plots an optimization “trajectory” for a  $S_0/S_1$  MECP of ethylene. Nine times within the first 14 optimization steps, the assignment of spin multiplicity becomes ambiguous in the sense that nominal “triplet” states possess  $\langle \hat{S}^2 \rangle$  values similar to those for the “singlet” states. (For the purpose of this calculation, we assume that any state with  $\langle \hat{S}^2 \rangle < 1.5$  is a singlet). Mixing of singlet and

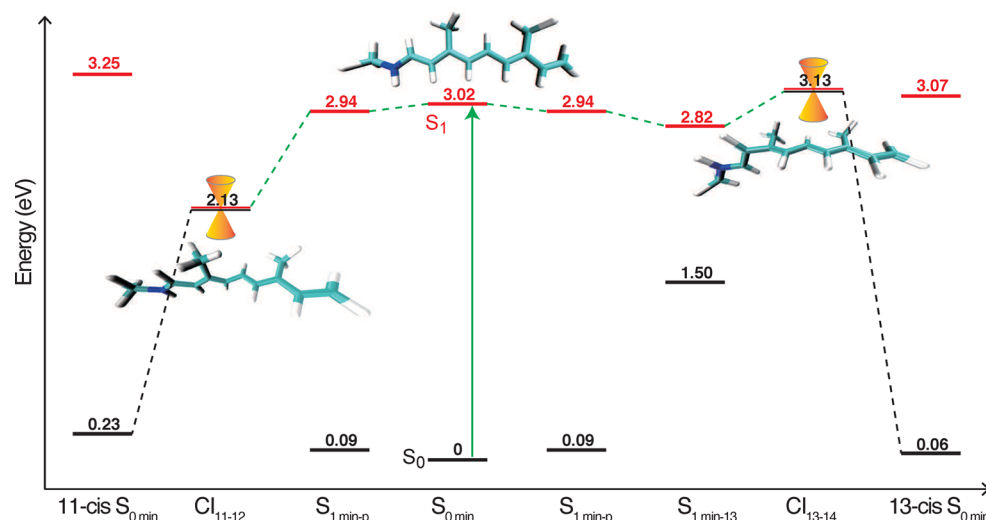


**Figure 7.** Energy level diagram for isomerization about either the  $\text{C}_{11}=\text{C}_{12}$  or  $\text{C}_{13}=\text{C}_{14}$  bond for an all-*trans* RPSB analogue. Results were computed using SF-TDDFT at the BH&HLYP/6-31G\* level.  $S_{1\text{min-p}}$  is a planar  $S_1$  minimum and  $S_{1\text{min-13}}$  is a minimum that is twisted about the  $\text{C}_{13}=\text{C}_{14}$  bond.

triplet spin components leads to an oscillatory trajectory that takes many steps to converge. This behavior is unacceptable in molecular dynamics applications, and in such cases one must resort to state-tracking techniques that attempt to assign spin multiplicity based on overlap with the wave function at the previous step.<sup>21,29</sup>

Recently, we reported a spin-adapted (SA) version of SF-TDDFT that we call SA-SF-DFT.<sup>21</sup> This approach automatically generates the minimum number of additional determinants required to construct proper  $S^2$  eigenstates, for example, the missing configurations in Figure 2c–e. As a result,  $S$  is restored as a good quantum number and spin multiplicity is well-defined. Figure 8b shows the SA-SF-DFT optimization trajectory for the same MECP of ethylene. Rapid oscillations are significantly reduced, the optimization reaches the correct intersection seam within six steps, and the overall number of steps to converge the MECP is reduced significantly.

### 3. EXCITON MODELS

Molecular excitons, that is, collective excitations in multi-chromophore systems, represent an important class of excited-state problems. Examples include the light-harvesting complexes of plants and photosynthetic bacteria, for which there is an ongoing debate about the role of quantum coherence in the energy-transfer dynamics,<sup>30,31</sup> an issue that also arises in studies of conjugated organic polymers.<sup>32</sup> Another important example is the singlet fission phenomenon,<sup>5</sup> in which triplet states on two chromophores spin-couple to a singlet but then diffuse apart, generating two charge carriers per photon.

In these examples, even the individual chromophores are not small by quantum chemistry standards, and *ab initio* calculations of energy transfer in large arrays of chromophores quickly become intractable. Nevertheless, semiempirical studies suggest that treatment of the extended chromophore array can have a profound effect on the simulated energy-transfer dynamics.<sup>33</sup>

#### 3.1. Frenkel–Davydov Exciton Model

An old idea for obtaining a qualitative understanding of the nature of collective excitations in systems of coupled chromophores is the Frenkel–Davydov exciton model, in which the wave functions  $|\Psi_n\rangle$  for the collective system are expanded in a basis of monomer excitations:<sup>34</sup>

$$|\Psi_n\rangle = \sum_A^{\text{monomers}} C_n^A \left( |\psi_A^*\rangle \prod_{B \neq A} |\psi_B\rangle \right) \quad (8)$$

Here,  $|\psi_B\rangle$  represents the ground-state wave function for monomer  $B$  and  $|\psi_A^*\rangle$  is an excited-state wave function for monomer  $A$ . The Hamiltonian matrix is then constructed and diagonalized in a basis

$$|\psi_A^*\psi_B\psi_C\dots\rangle, |\psi_A\psi_B^*\psi_C\dots\rangle, \dots$$

whose dimension is simply the number of monomers, in order to determine the coefficients  $C_n^A$  in eq 8. This “exciton site basis” can be envisaged as a natural set of diabatic states in which to represent the adiabatic states  $|\Psi_n\rangle$ .

Construction of the Hamiltonian requires matrix elements of  $\hat{H}$  in the exciton site basis. Historically (but even in modern implementations<sup>35,36</sup>), this has been accomplished using dipole-coupling approximations or by evaluating the Coulomb integral between transition densities on different sites.<sup>37–39</sup> Both approaches neglect exchange coupling between the monomers. In contrast, we have recently reported an *ab initio* Frenkel–Davydov exciton

model (AIFDEM) that avoids these approximations,<sup>34,40</sup> and thus seeks a quantitative description of excitation energy transfer while maintaining the intuitive appeal (and trivial parallelizability) of the original model.

Our model assumes that the excited monomer wave functions  $|\psi_X^*\rangle$  are linear combinations of singly excited Slater determinants  $|\Phi_X^{ia}\rangle$ , as in eq 1. These can be efficiently computed for isolated monomers in a distributed fashion, as can coupling matrix elements such as

$$\begin{aligned} H_{AB} &= \langle \psi_A^* \psi_B \psi_C \dots | \hat{H} | \psi_A \psi_B^* \psi_C \dots \rangle \\ &= \sum_{ia\sigma} \sum_{jb\tau} t_{ia\sigma}^A t_{jb\tau}^B \langle \Phi_A^{ia} \Phi_B^{jb} \Phi_C \dots | \hat{H} | \Phi_A \Phi_B^{jb} \Phi_C \dots \rangle \end{aligned} \quad (9)$$

and overlap integrals

$$S_{AB} = \langle \psi_A^* \psi_B \psi_C \dots | \psi_A \psi_B^* \psi_C \dots \rangle \quad (10)$$

that are necessary because the monomer CIS or TDDFT calculations are carried out independently of the other chromophores; thus the orbitals on different monomers are not orthogonal. (The spin indices  $\sigma$  and  $\tau$  in eq 9 are a shorthand notation to imply that we construct proper spin eigenstates<sup>34</sup>). Notably,  $\hat{H}$  is the full electronic Hamiltonian for the aggregate; hence no dipole-coupling, neglect-of-exchange, or nearest-neighbor approximation has been made. The method affords a well-defined wave function for the supersystem, so that properties such as oscillator strengths are straightforward to compute.

Having constructed the matrix elements in eqs 9 and 10, the AIFDEM then consists of solving the Schrödinger equation  $\mathbf{H}\mathbf{C} = \mathbf{E}\mathbf{S}\mathbf{C}$ , and we find that the eigenvalues  $E$  tend to lie within ~0.2 eV of the results of a supersystem CIS calculation.<sup>34,40</sup> This is true even for challenging test cases such as chains of He atoms, where the excited states resemble particle-in-a-box states that are maximally delocalized across monomers. In such cases, it is necessary to increase the variational flexibility of the direct-product basis by including more than one excited state per monomer ( $|\psi_A^*\psi_B\psi_C\dots\rangle$ , etc.), but this adds very little to the computational cost. The basis can be further augmented with “charge resonance” determinants, for example,  $|\psi_A^+\psi_B^-\psi_C\dots\rangle$  and  $|\psi_A^-\psi_B^+\psi_C\dots\rangle$ .

As originally formulated in eq 9, the cost to evaluate matrix elements grows as the fourth power of supersystem size, which is necessary to capture the nonlocal exchange interaction. This interaction is short-ranged, however, and in fact only those monomers nearby the excited monomers ( $A$  and  $B$  in the matrix element shown in eq 9) need to be treated quantum-mechanically, in order to capture the Pauli repulsion that is responsible for “Rydbergization”<sup>41</sup> of the monomer excited states. The remaining monomers can be replaced with point charges that capture the long-range Coulomb interactions.<sup>40</sup> This affords an algorithm whose cost scales only quadratically with the number of fragments and can outperform a traditional calculation by as much as 200× even in modest calculations involving <10 monomers.<sup>40</sup>

Due to the nearly perfect parallel efficiency of the AIFDEM, however, we are able to perform calculations on much larger aggregates that would be intractable by other means. Consider, for example, the self-assembling naphthalene diimide (NDI) nanotube shown in Figure 9b, for which an atomistic structural model was recently reported.<sup>42</sup> This material is an organic semiconductor, and even the small (NDI)<sub>9</sub> substructure shown in Figure 9c exhibits a dense manifold of excited states, with the

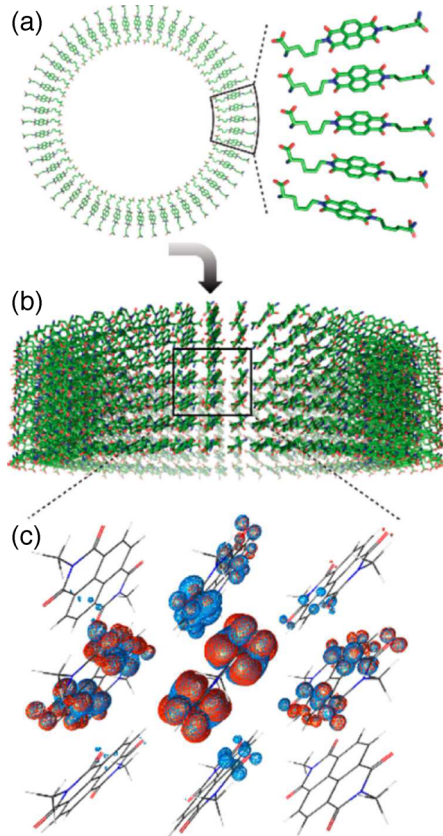


**Figure 9.** Structural model of a NDI-lysine nanotube, showing (a) the monomers and how they are arranged into rings, (b) the full nanotube structural model, and (c) a methylated (NDI)<sub>9</sub> substructure and a TDDFT/3-21G\* calculation of its lowest bright state ( $S_{27}$ ). Reprinted with permission from ref 42. Copyright 2015 American Chemical Society.

lowest bright state as  $S_{27}$  and energy gaps of  $\sim 0.05$  eV.<sup>42</sup> It is unclear from the TDDFT calculation in Figure 9c whether the extent of exciton delocalization has been captured in this nine-unit model, but already this system taxes our ability to perform TDDFT calculations on commodity hardware. For example, we estimate that  $\gtrsim 30$  Gb of memory would be required to increase the basis set from 3-21G\* to 6-31+G\*.<sup>40</sup>

The memory footprint of the AIFDEM, in contrast, is no larger than that of a CIS calculation on a pair of monomers. Moreover, the parallel scalability allows us to treat an unprecedented number of chromophores from first principles. Table 2 lists the

**Table 2. Resources Required to Perform an AIFDEM/6-31G\* Calculation in <1 Week on (NDI)<sub>N</sub> Nanotube Substructures**

<i>N</i>	no. basis functions	no. processors
2	700	3
4	1400	10
9	3150	20
42	14 700	150
156	54 600	440

Reprinted with permission from ref 40. Copyright 2015 American Chemical Society.

size of various (NDI)<sub>N</sub> substructures for which an AIFDEM calculation requires less than 1 week of wall time on the indicated number of processors. For the largest of these calculations, the equivalent supersystem TDDFT calculation would involve

54 600 basis functions, yet the AIFDEM calculation finishes in <1 week on only 440 processors.<sup>40</sup> It is significant that each of the calculations in Table 2 could be performed in a matter of days on a laboratory computer cluster, rather than a supercomputer.

The exciton Hamiltonian matrix  $\mathbf{H}$  can be used to propagate either the time-dependent Schrödinger equation or else some dissipative master equation representing interactions with a phonon bath. We choose the latter approach, applying Redfield's equation<sup>43</sup> to simulate the quantum dynamics of excitation energy transfer in two different nanotube substructures: (NDI)<sub>9</sub> and (NDI)<sub>42</sub>. Starting from an excitation that is localized on a single chromophore and that is therefore not an eigenstate of  $\mathbf{H}$ , we plot in Figure 10 how the excitation energy is rapidly scrambled between monomers. The overall dynamics is guided by static disorder, and the excitation rapidly localizes on sites that are energetically favorable. The fact that small fluctuations in site energies may significantly impact the dynamics underscores the importance of an atomistic, first-principles description of the energetics, as an alternative to empirical exciton models. Interestingly, we find that coherent oscillations persist to much longer time scales in the larger model, as a result of a larger number of resonant site energies, whereas in the smaller (NDI)<sub>9</sub> model there are more significant "edge effects" that lead to rapid dephasing.<sup>40</sup> It is possible that a more rigorous treatment of static disorder (i.e., including nuclear degrees of freedom in the dynamics) might suppress these coherences in (NDI)<sub>42</sub>, but the edge effects and concomitant differences in the distribution of site energies are likely to remain. As such, this example serves to illustrate that qualitatively different site energies and couplings can be obtained if the size of the model system is pushed well beyond what can be simulated using traditional supersystem methods.

### 3.2. Approximations to TDDFT

Although the AIFDEM sits outside of conventional TDDFT, it is also possible to apply exciton-type ideas within the framework of TDDFT, in order to reduce its cost for systems composed of weakly interacting molecules. Our approach can be considered an excited-state extension of the "self-consistent field for molecular interactions" [SCF(MI)] procedure,<sup>44</sup> which employs "absolutely localized" MOs, such that MOs on a particular monomer are formed from linear combinations of atom-centered Gaussian basis functions on the same monomer. When the number of monomers is large, this significantly speeds up the ground-state SCF calculation.<sup>44</sup>

To develop a "TDDFT(MI)" procedure,<sup>45</sup> we invoke an additional *ansatz* in which the transition density  $\delta\hat{\rho}$  is expressed as a linear combination of one or more excitations localized on each monomer:

$$\begin{aligned} \delta\hat{\rho} &= \sum_F^{\text{monomers}} \sum_n^{\text{roots}} \Theta_{F,n} \delta\hat{\rho}_{F,n} \\ &= \sum_F^{\text{monomers}} \sum_n^{\text{roots}} \Theta_{F,n} \left( \sum_{ai \in F} X_{ai}^{(F,n)} |\phi_a\rangle \langle \phi_i| \right) \end{aligned} \quad (11)$$

The  $X_{ai}^{(F,n)}$  are TDDFT transition amplitudes for the *n*th excited state of monomer *F*. From eq 11 follows a set of equations for the coefficients  $\Theta_{F,n}$  and the supersystem excitation energy,  $\omega$ :<sup>45</sup>

$$\begin{aligned} &\sum_G^{\text{monomers}} \sum_m^{\text{roots}} (\mathbf{X}^{(F,n)})^\dagger \mathbf{A}^{(F,G)} \mathbf{X}^{(G,m)} \Theta_{G,m} \\ &= \omega \sum_G^{\text{monomers}} \sum_m^{\text{roots}} (\mathbf{X}^{(F,n)})^\dagger \Delta^{(F,G)} \mathbf{X}^{(G,m)} \Theta_{G,m} \end{aligned} \quad (12)$$

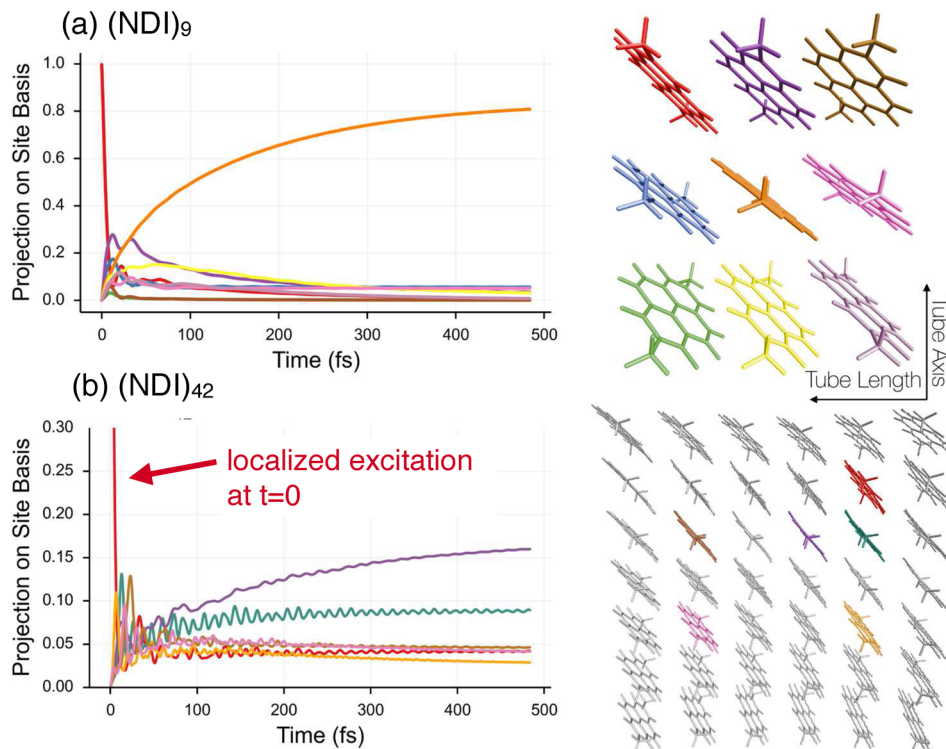


**Figure 10.** Redfield dynamics<sup>43</sup> of (a) (NDI)<sub>9</sub>, and (b) (NDI)<sub>42</sub> substructures extracted from the nanotube in Figure 9b. Plotted are the populations of individual exciton-site basis states as the initially localized excitation evolves in time. The populations are color-coded to the structural models on the right. Reprinted with permission from ref 40. Copyright 2015 American Chemical Society.

The matrix  $\mathbf{A}^{(F,G)}$  is the usual TDDFT orbital Hessian,<sup>2</sup> consisting in part of two-electron integrals ( $ia||jb$ ). However,  $A_{ai,bj}^{(F,G)}$  consists of only those matrix elements such that  $ai \in F$  and  $bj \in G$ . In TDDFT(MI), there is no need to evaluate two-electron integrals with more than two molecular centers, leading to significant savings. The quantity  $\Delta_{ai,bj}^{(F,G)} = S_{ab}S_{ij}$  in eq 12 is an overlap that accounts for the fact that the MOs on different monomers are not orthogonal. Some additional localization approximations are also employed, as described in previous work.<sup>45,46</sup>

Even for cases of a collective excitation delocalized over multiple monomer units, such as the NDI aggregates considered above, we find that TDDFT(MI) reproduces supersystem TDDFT excitation energies to within  $\sim 0.2$  eV, as shown in Table 3. As with the AIFDEM, the monomer calculations are

trivially parallelizable, and for TDDFT(MI) the dimension of eq 12 equals the number of monomers times the number of roots per monomer, where the latter can be increased to improve the flexibility of the *ansatz* in eq 11. Timing data in Figure 11

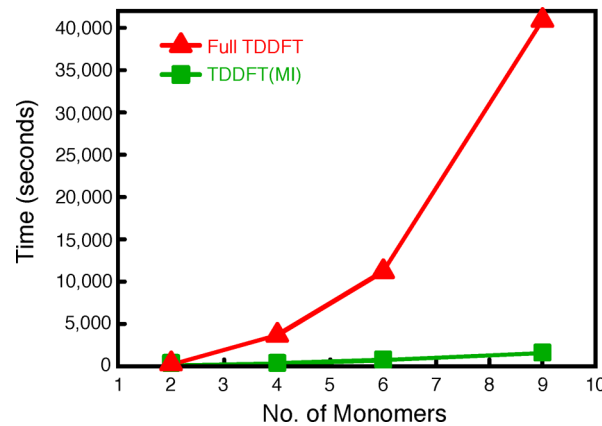


**Figure 11.** Timings for (NDI)<sub>N</sub> aggregates at the CIS/6-31G level. All calculations were multithreaded across 20 processors.

**Table 3. Excitation Energies<sup>a</sup> for Methylated (NDI)<sub>N</sub> Substructures of the Nanotube in Figure 9b**

N	state <sup>b</sup>	excitation energy (eV)		
		TDDFT(MI)	TDDFT	diff
4	T <sub>1</sub>	1.796	1.778	0.018
	S <sub>1</sub>	4.091	4.047	0.044
	S <sub>b</sub>	4.393	4.270	0.123
6	T <sub>1</sub>	1.796	1.755	0.041
	S <sub>1</sub>	4.076	3.990	0.086
	S <sub>b</sub>	4.469	4.267	0.202
9	T <sub>1</sub>	1.785	1.737	0.048
	S <sub>1</sub>	4.070	3.970	0.100
	S <sub>b</sub>	4.537	4.300	0.237

Adapted with permission from ref 45. Copyright 2015 American Chemical Society. <sup>a</sup>LRC- $\omega$ PBE functional. <sup>b</sup>Lowest triplet (T<sub>1</sub>), lowest singlet (S<sub>1</sub>), and lowest dipole-allowed excitation (S<sub>b</sub>).

demonstrate the dramatic reduction in cost compared with a full (supersystem) TDDFT calculation.

A particularly efficient scenario occurs when the excitation can be assumed to be localized on a single monomer, as in the case of a single chromophore in the presence of a large number of explicit solvent molecules. In this case, one may neglect all terms in eq 12 where  $F \neq G$ , and the TDDFT calculation need only be performed on the chromophore.<sup>45,46</sup> The cost of the TDDFT calculation is therefore independent of the number of solvent molecules, allowing environmental effects on the excitation

to be tractably converged by making the supersystem as large as possible.

Whereas TDDFT calculations in explicit solvent are ordinarily beset by a sea of spurious charge-transfer-to-solvent states,<sup>47,48</sup> such states are absent in the TDDFT(MI) approach because the amplitudes  $X_{ai}$  that would support them are omitted. We therefore anticipate that TDDFT(MI) excitation energies may converge faster than conventional TDDFT ones with respect to the number of solvent molecules. This is demonstrated in Figure 12 for

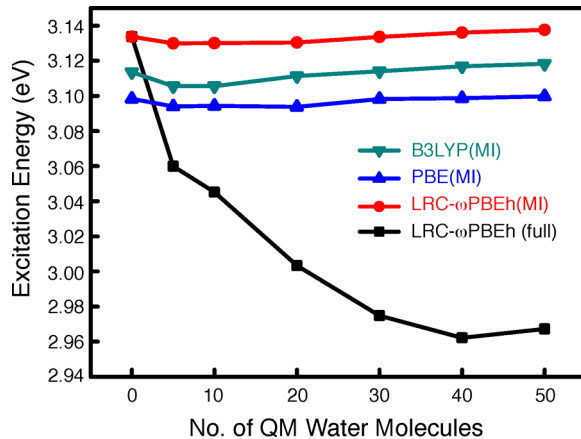


**Figure 12.**  $S_0 \rightarrow S_1$  excitation energies of  $pCT^-$ , including an increasingly large number of quantum-mechanical water molecules, with additional classical water molecules for a total of 994 solvent molecules. All calculations use the TDDFT(MI) approach except for the “full” (supersystem) calculation, and the basis is 6-31G\*.

the  $S_0 \rightarrow S_1$  excitation of *trans*-thiophenyl-*p*-coumarate ( $pCT^-$ ), a model of the chromophore in yellow fluorescent protein. TDDFT(MI) excitation energies converge quickly, whereas in the supersystem calculation the  $S_0 \rightarrow S_1$  excitation energy drops precipitously as the number of solvent molecules increases, because larger systems engender more numerous (but ultimately spurious) charge-transfer states.

#### 4. LOOKING TO THE FUTURE

Whereas most detailed quantum-chemical studies of the dynamics near CIs have used expensive multireference wave function models, the availability of analytic derivative couplings for the relatively low-cost SF-TDDFT approach enables such studies in much larger molecules. Importantly, the spin-flip approach affords a more balanced description of ground and excited states, as compared with conventional TDDFT, and correctly describes the topology in the vicinity of a CI. We expect to see many SF-TDDFT studies of photochemical reactions in the near future, with the caveat that significant spin contamination often necessitates the use of state-tracking algorithms in order to maintain the dynamics or geometry optimization on a state with consistent spin multiplicity.<sup>21,29</sup> A “spin-complete” implementation that restores proper spin eigenstates has been developed by our group but presently lacks the analytic energy gradients that are required for routine application to geometry optimizations and molecular dynamics.<sup>21</sup>

While SF-TDDFT is formulated in a general way for application to arbitrary molecular systems, additional savings can be realized for certain classes of problems, including those containing multiple, electronically coupled chromophores. Our *ab initio* exciton model offers a promising framework for systems where the collective nature (and dense manifold) of excited

states means that realistic model systems are often too large even for TDDFT. While the present version of the AIFDEM can describe entangled excitations between monomers, such as the “multi-exciton” state in singlet fission,<sup>5</sup> in future work we hope to report on a version of the AIFDEM that also includes electron correlation on the monomers, in order to obtain more accurate site energies. Moreover, formulation of analytic gradients of the coupling matrix elements in eq 9 will facilitate studies of how excitation energy transfer depends upon inter- and intramolecular vibrational modes.

Excitonic approximations within TDDFT itself, in what we call the TDDFT(MI) approach,<sup>45,46</sup> can also describe coupled chromophores at dramatically reduced cost. TDDFT(MI) is particularly attractive for obtaining converged solvatochromatic shifts, or shifts in excitation energies due to embedding in a protein matrix, at a cost whose wall time grows very slowly with system size.

All of the methods described herein are available in version 4.4 of the Q-CHEM software package.<sup>9</sup>

#### ■ AUTHOR INFORMATION

##### Corresponding Author

\*E-mail: [herbert@chemistry.ohio-state.edu](mailto:herbert@chemistry.ohio-state.edu).

##### Present Address

<sup>‡</sup>J.L.: Max-Planck-Institut für Kohlenforschung, Kaiser-Wilhelm-Platz 1, 45470 Mülheim an der Ruhr, Germany

##### Notes

The authors declare the following competing financial interest(s): J.M.H. serves on the Board of Directors of Q-Chem, Inc.

#### Biographies

**John Herbert** obtained his Ph.D. from the University of Wisconsin in 2003, joined The Ohio State University as an Assistant Professor in 2006, and was promoted to Associate Professor in 2011 and then to Professor in 2014. His research group is a major contributor to the Q-CHEM electronic structure program.

**Xing Zhang** graduated from Nanjing University in 2011. As a Ph.D. student with Prof. Herbert, he focuses on TDDFT and related methods for computational photochemistry.

**Adrian Morrison** received a B.A. in chemistry from Ohio Wesleyan University in 2012 and is currently a Ph.D. student in Prof. Herbert’s group, working on methods for excited states and high-performance computing.

**Jie Liu** obtained his Ph.D. from the University of Science and Technology of China in 2012 under the supervision of Prof. WanZhen Liang. Following postdoctoral work with Prof. Herbert, where he worked on TDDFT and fragment-based quantum chemistry, in 2016 he joined Prof. Walter Thiel’s group at the Max Planck Institute für Kohlenforschung in Mülheim an der Ruhr, Germany.

#### ■ ACKNOWLEDGMENTS

Work on derivative couplings was supported by the National Science Foundation, Division of Chemistry (Grant No. CHE-1300603). Work on exciton models was supported by the Department of Energy, Office of Basic Energy Sciences, Division of Chemical Sciences, Geosciences, and Biosciences (Award No. DE-SC0008550). Calculations were performed at the Ohio Supercomputer Center (Project No. PAA-0003).<sup>49</sup> J.M.H. is a Camille Dreyfus Teacher-Scholar and a fellow of the Alexander von Humboldt Foundation.

## ■ REFERENCES

- (1) Mencken, H. L. *A Mencken Chrestomathy*; Alfred A. Knopf: New York, 1949; Chapter 25, p 443.
- (2) Dreuw, A.; Head-Gordon, M. Single-reference ab initio methods for the calculation of excited states of large molecules. *Chem. Rev.* **2005**, *105*, 4009–4037.
- (3) Silva-Junior, M. R.; Schreiber, M.; Sauer, S. P. A.; Thiel, W. Benchmarks for electronically excited states: Time-dependent density functional theory and density functional theory based multireference configuration interaction. *J. Chem. Phys.* **2008**, *129*, 104103.
- (4) Rohrdanz, M. A.; Martins, K. M.; Herbert, J. M. A long-range-corrected density functional that performs well for both ground-state properties and time-dependent density functional theory excitation energies, including charge-transfer excited states. *J. Chem. Phys.* **2009**, *130*, 054112.
- (5) Smith, M. B.; Michl, J. Recent advances in singlet fission. *Annu. Rev. Phys. Chem.* **2013**, *64*, 361–386.
- (6) Levine, B. G.; Ko, C.; Quenneville, J.; Martínez, T. J. Conical intersections and double excitations in time-dependent density functional theory. *Mol. Phys.* **2006**, *104*, 1039–1051.
- (7) Zhang, X.; Herbert, J. M. Analytic derivative couplings for spin-flip configuration interaction singles and spin-flip time-dependent density functional theory. *J. Chem. Phys.* **2014**, *141*, 064104.
- (8) Zhang, X.; Herbert, J. M. Analytic derivative couplings in time-dependent density functional theory: Quadratic response theory versus pseudo-wavefunction approach. *J. Chem. Phys.* **2015**, *142*, 064109.
- (9) Krylov, A. I.; Gill, P. M. W. Q-Chem: An engine for innovation. *WIREs Comput. Mol. Sci.* **2013**, *3*, 317–326.
- (10) Shao, Y.; Head-Gordon, M.; Krylov, A. I. The spin-flip approach within time-dependent density functional theory: Theory and applications to diradicals. *J. Chem. Phys.* **2003**, *118*, 4807–4818.
- (11) Paterson, M. J.; Robb, M. A.; Blancafort, L.; DeBellis, A. D. Mechanism of an exceptional class of photostabilizers: A seam of conical intersection parallel to excited state intramolecular proton transfer (ESIPT) in *o*-hydroxyphenyl-(1,3,5)-triazine. *J. Phys. Chem. A* **2005**, *109*, 7527–7537.
- (12) Yarkony, D. R. Diabolical conical intersections. *Rev. Mod. Phys.* **1996**, *68*, 985–1013.
- (13) Matsika, S.; Krause, P. Nonadiabatic events and conical intersections. *Annu. Rev. Phys. Chem.* **2011**, *62*, 621–643.
- (14) Atchity, G. J.; Xantheas, S. S.; Ruedenberg, K. Potential energy surfaces near intersections. *J. Chem. Phys.* **1991**, *95*, 1862–1876.
- (15) Yarkony, D. R. Nuclear dynamics near conical intersections in the adiabatic representation: I. The effects of local topography on interstate transitions. *J. Chem. Phys.* **2001**, *114*, 2601.
- (16) Ben-Nun, M.; Molnar, F.; Schulten, K.; Martínez, T. J. The role of intersection topography in bond selectivity of *cis-trans* photoisomerization. *Proc. Natl. Acad. Sci. U. S. A.* **2002**, *99*, 1769–1773.
- (17) Virshup, A. M.; Chen, J.; Martínez, T. J. Nonlinear dimensionality reduction for nonadiabatic dynamics: The influence of conical intersection topography on population transfer rates. *J. Chem. Phys.* **2012**, *137*, 22A519.
- (18) Send, R.; Furche, F. First-order nonadiabatic couplings from time-dependent hybrid density functional response theory: Consistent formalism, implementation, and performance. *J. Chem. Phys.* **2010**, *132*, 044107.
- (19) Li, Z.; Suo, B.; Liu, W. First-order nonadiabatic coupling matrix elements between excited states: Implementation and application at the TD-DFT and pp-TDA levels. *J. Chem. Phys.* **2014**, *141*, 244105.
- (20) Subotnik, J. E.; Alguire, E. C.; Ou, Q.; Landry, B. R.; Fatehi, S. The requisite electronic structure theory to describe photoexcited non-adiabatic dynamics: Nonadiabatic derivative couplings and diabatic electronic couplings. *Acc. Chem. Res.* **2015**, *48*, 1340–1350.
- (21) Zhang, X.; Herbert, J. M. Spin-flip, tensor equation-of-motion configuration interaction with a density-functional correction: A spin-complete method for exploring excited-state potential energy surfaces. *J. Chem. Phys.* **2015**, *143*, 234107.
- (22) Huix-Rotllant, M.; Natarajan, B.; Ipatov, A.; Wawire, C. M.; Deutsch, T.; Casida, M. E. Assessment of noncollinear spin-flip Tamm-Dancoff approximation time-dependent density-functional theory for the photochemical ring-opening of oxirane. *Phys. Chem. Chem. Phys.* **2010**, *12*, 12811–12825.
- (23) Minezawa, N.; Gordon, M. S. Optimizing conical intersections by spin-flip density functional theory: Application to ethylene. *J. Phys. Chem. A* **2009**, *113*, 12749–12753.
- (24) Minezawa, N.; Gordon, M. S. Photoisomerization of stilbene: A spin-flip density functional theory study. *J. Phys. Chem. A* **2011**, *115*, 7901–7911.
- (25) Zhang, X.; Herbert, J. M. Excited-state relaxation pathways in uracil versus hydrated uracil: Solvatochromatic shift in the  ${}^1n\pi^*$  state is the key. *J. Phys. Chem. B* **2014**, *118*, 7806–7817.
- (26) Ernst, O. P.; Lodowski, D. T.; Elstner, M.; Hegemann, P.; Brown, L. S.; Kandori, H. Microbial and animal rhodopsins: Structures, functions, and molecular mechanisms. *Chem. Rev.* **2014**, *114*, 126–163.
- (27) Wand, A.; Gdor, I.; Zhu, J.; Sheves, M.; Ruhman, S. Shedding new light on retinal protein photochemistry. *Annu. Rev. Phys. Chem.* **2013**, *64*, 437–458.
- (28) Gozem, S.; Huntress, M.; Schapiro, I.; Lindh, R.; Granovsky, A. A.; Angeli, C.; Olivucci, M. Dynamic electron correlation effects on the ground state potential energy surface of a retinal chromophore model. *J. Chem. Theory Comput.* **2012**, *8*, 4069–4080.
- (29) Harabuchi, Y.; Keipert, K.; Zahariev, F.; Taketsugu, T.; Gordon, M. S. Dynamics simulations with spin-flip time-dependent density functional theory: Photoisomerization and photocyclization mechanisms of *cis*-stilbene in  $\pi\pi^*$  states. *J. Phys. Chem. A* **2014**, *118*, 11987–11998.
- (30) Kassal, I.; Yuen-Zhou, J.; Rahimi-Keshari, S. Does coherence enhance transport in photosynthesis? *J. Phys. Chem. Lett.* **2013**, *4*, 362–367.
- (31) Chenu, A.; Scholes, G. D. Coherence in energy transfer and photosynthesis. *Annu. Rev. Phys. Chem.* **2015**, *66*, 69–96.
- (32) Hwang, I.; Scholes, G. D. Electronic energy transfer and quantum-coherence in  $\pi$ -conjugated polymers. *Chem. Mater.* **2011**, *23*, 610–620.
- (33) Olbrich, C.; Jansen, T. L. C.; Liebers, J.; Strümpfer, J.; Schulten, K.; Knoester, J.; Kleinekathöfer, U.; Aghtar, M. From atomistic modeling to excitation transfer and two-dimensional spectra of the FMO light-harvesting complex. *J. Phys. Chem. B* **2011**, *115*, 8609–8621.
- (34) Morrison, A. F.; You, Z.-Q.; Herbert, J. M. Ab initio implementation of the Frenkel-Davydov exciton model: A naturally parallelizable approach to computing collective excitations in crystals and aggregates. *J. Chem. Theory Comput.* **2014**, *10*, 5366–5376.
- (35) Bouvier, B.; Gustavsson, T.; Markovitsi, D.; Millié, P. Dipolar coupling between electronic transitions of the DNA bases and its relevance to exciton states in double helices. *Chem. Phys.* **2002**, *275*, 75–92.
- (36) Bouvier, B.; Dognon, J.-P.; Lavery, R.; Markovitsi, D.; Millié, P.; Onidas, D.; Zakrzewska, K. Influence of conformational dynamics on the exciton states of DNA oligomers. *J. Phys. Chem. B* **2003**, *107*, 13512–13522.
- (37) Krueger, B. P.; Scholes, G. D.; Fleming, G. R. Calculation of couplings and energy-transfer pathways between the pigments of LH2 by the ab initio transition density cube method. *J. Phys. Chem. B* **1998**, *102*, 5378–5386.
- (38) Tretiak, S.; Zhang, W. M.; Chernyak, V.; Mukamel, S. Excitonic couplings and electronic coherence in bridged naphthalene dimers. *Proc. Natl. Acad. Sci. U. S. A.* **1999**, *96*, 13003–13008.
- (39) Czader, A.; Bittner, E. R. Calculations of the exciton coupling elements between the DNA bases using the transition density cube method. *J. Chem. Phys.* **2008**, *128*, 035101.
- (40) Morrison, A. F.; Herbert, J. M. Low-scaling quantum chemistry approach to excited-state properties via an ab initio exciton model: Application to excitation energy transfer in a self-assembled nanotube. *J. Phys. Chem. Lett.* **2015**, *6*, 4390–4396.
- (41) Mulliken, R. S. Rydberg states and Rydbergization. *Acc. Chem. Res.* **1976**, *9*, 7–12.
- (42) Gao, M.; Paul, S.; Schwieters, C. D.; You, Z.-Q.; Shao, H.; Herbert, J. M.; Parquette, J. R.; Jaroniec, C. P. An atomic resolution

structural model for a self-assembled nanotube provides insight into its exciton dynamics. *J. Phys. Chem. C* **2015**, *119*, 13948–13956.

(43) Pollard, W. T.; Felts, A. K.; Friesner, R. A. The Redfield equation in condensed-phase quantum dynamics. *Adv. Chem. Phys.* **1996**, *93*, 77–134.

(44) Khaliullin, R. Z.; Head-Gordon, M.; Bell, A. T. An efficient self-consistent field method for large systems of weakly-interacting fragments. *J. Chem. Phys.* **2006**, *124*, 204105.

(45) Liu, J.; Herbert, J. M. An efficient and accurate approximation to time-dependent density functional theory for systems of weakly coupled monomers. *J. Chem. Phys.* **2015**, *143*, 034106.

(46) Liu, J.; Herbert, J. M. Local excitation approximations to time-dependent density functional theory for excitation energies in solution. *J. Chem. Theory Comput.* **2016**, *12*, 157–166.

(47) Lange, A.; Herbert, J. M. Simple methods to reduce charge-transfer contamination in time-dependent density-functional calculations of clusters and liquids. *J. Chem. Theory Comput.* **2007**, *3*, 1680–1690.

(48) Isborn, C. M.; Mar, B. D.; Curchod, B. F. E.; Tavernelli, I.; Martínez, T. J. The charge transfer problem in density functional theory calculations of aqueously solvated molecules. *J. Phys. Chem. B* **2013**, *117*, 12189–12201.

(49) Ohio Supercomputer Center, <http://osc.edu/ark:/19495/f5s1ph73>.